Received: 2 June 2024 | Accepted: 5 July 2024

DOI: 10.1111/srt.13871

ORIGINAL ARTICLE

WILEY

Identification of shared immune infiltration characteristic molecules in dermatomyositis and nasopharyngeal carcinoma using bioinformatics

Traits in dermatomyositis and nasopharyngeal cancer

Jinyan Kai[1] | **Haitao Huang**[2] | **Jiaqi Su**[1] | **Qiong Chen**[3]

[1]Department of Clinical Medical Laboratory, The Affiliated Second Hospital of Xiamen Medical College, Xiamen, Fujian, China

[2]Department of Microbiology, Guilin Medical University, Guilin, Guangxi, China

[3]Department of Traditional Chinese Medicine, Shanghai General Hospital, School of Medicine, Shanghai Jiao Tong University, Shanghai, China

Correspondence
Qiong Chen, Department of Traditional Chinese Medicine, Shanghai General Hospital, School of Medicine, Shanghai Jiao Tong University, Shanghai, China.
Email: chenqiongjone@163.com

Abstract

Background: Dermatomyositis (DM) is a kind of dermatologically associated autoimmune disease that is notably associated with an increased risk of concurrent malignancies, although the underlying mechanisms remain to be fully elucidated. The purpose of this investigation was to examine the immunological parallels between DM and nasopharyngeal carcinoma (NPC), with the aim of identifying pivotal biomarkers that could facilitate a deeper understanding and enhance the predictive capabilities of NPC in DM patients.

Method: Data for DM and NPC were sourced from the Gene Expression Omnibus (GEO) database. Immune infiltration was analyzed using the "cibersort" R package, differentially expressed genes (DEGs) were identified with the "limma" package, and functional pathways were investigated through Kyoto Encyclopedia of Genes and Genomes (KEGG) and Gene Ontology (GO) analyses. Characteristic genes were determined by Utilizing Protein–Protein Interaction (PPI) and Least Absolute Shrinkage and Selection Operator (LASSO), and their features were validated using the GSE53819 dataset.

Results: In comparison to normal samples, significant infiltration of macrophage M1 was observed in both DM and NPC. The analysis revealed 77 DEGs in DM and 1051 DEGs in NPC, with 22 genes found to be co-DEGs. Following PPI and LASSO analysis, six distinctive genes were retained. Notably, CCL8, IFIH1, CXCL10, and CXCL11 exhibited optimal diagnostic efficacy for NPC and displayed significant correlation with macrophage M1 infiltration within the carcinoma.

Conclusion: Four characteristic genes, CCL8, IFIH1, CXCL10, and CXCL11 are risk factors for both DM and NPC. They exhibit a robust correlation with the incidence of NPC and offer a commendable diagnostic efficacy. Furthermore, they may serve as prospective predictive biomarkers for the emergence of NPC in DM.

Jinyan Kai and Haitao Huang contributed to the work equally and should be regarded as co-first authors.

KEYWORDS
bioinformatics, dermatomyositis, differentially expressed genes, nasopharyngeal carcinoma

1 | INTRODUCTION

Dermatomyositis (DM) is a dermatologically associated systemic inflammatory disease that affects both children and adults, manifesting with characteristic skin manifestations and significant muscle weakness.[1] Comorbidities or complications are more deadly factors in patients with DM. Because some studies have shown that the incidence of malignant tumors in patients with DM is significantly higher than that in the normal population within 1 year after diagnosis.[2,3] So far, the mechanism of malignant tumors in patients with DM is not clear.

Nasopharyngeal carcinoma (NPC) represents an epithelial malignancy arising within the nasopharyngeal region, exhibiting a strong etiological association with Epstein–Barr virus (EBV) infection.[4,5] The anatomical inaccessibility of the nasopharynx contributes to the advanced stage at which NPC is frequently detected, with approximately 70% of patients presenting at stages III or IV at the time of diagnosis.[6]

A hallmark characteristic of NPC is the abundant presence of immune cell infiltrates within the primary tumor microenvironment, comprising a diverse spectrum of immune constituents, including T lymphocytes, B lymphocytes, dendritic cells (DCs), monocytes, and eosinophils.[7] This rich inflammatory infiltrate suggests a complex interplay between the tumor and the host immune system.

NPC is among the most prevalent malignant neoplasms in Southeast China,[8] and it is also one of the main co-occurring malignancies of DM.[9,10] Given the rising incidence of DM in recent years, investigating the underlying mechanisms of DM complicated by NPC and delineating potential avenues for early intervention is critical for curbing the incidence of NPC.[8,11]

Bioinformatics is a current key approach for exploring tumor-related issues.[12] In light of this, the present study endeavored to use bioinformatics to scrutinize the potential interplay between the two pathologies from the perspective of immune microenvironment infiltration, thereby offering valuable insights to inform clinical diagnosis and therapeutic strategies for DM complicated by NPC. The flow diagram of the work is shown in Figure 1.

2 | MATERIALS AND METHODS

2.1 | Microarray datasets

The series matrix files and platform information were sourced from the Gene Expression Omnibus (GEO) database (https://www.ncbi.nlm.nih.gov/geo/).[13] Four gene expression profile datasets, namely GSE1551, GSE128470, GSE12452, and GSE53819, were retrieved via the "GEOquery" package.[14] GSE1551 and GSE128470 represent the gene expression profile datasets for DM, while GSE12452 and GSE53819 pertain to NPC. GSE1551 and GSE128470 were conducted on the GPL96 platform. GSE1551 comprises 13 DM samples and 10 normal controls, whereas GSE128470 consists of 12 DM samples and 12 normal controls. Given the limited sample size of DM in individual datasets, we opted to amalgamate the expression data from both DM datasets for subsequent analysis. GSE12452, utilizing the GPL570 platform, encompasses 31 NPC samples and 10 normal controls. GSE53819, employing the GPL6480 platform, comprises 18 NPC samples and 18 normal controls. Details of this dataset are given in Table 1.

2.2 | Identification of differentially expressed genes

The gene expression profiles and their matching platform files were imported into R software (version 4.1.1) for conversion into gene symbol expression profiles. The "limma" package[15] was utilized to identify differentially expressed genes (DEGs) between the disease group and the normal group, using the filtration standards referenced in this study,[16] with the criteria set at $|\log FC| > 1$ and $p < 0.05$. The online tool "Draw Venn Diagram" (http://bioinformatics.psb.ugent.be/webtools/Venn/) was employed to visualize the intersection of differentially expressed datasets, thereby identifying a common set of DEGs.

2.3 | Analysis of immune cell infiltration

CIBERSORT is a deconvolution algorithm designed to analyze gene expression data, leveraging gene expression signatures to quantify the relative abundance of various immune cell types. For assessing immune cell infiltration, we employed the CIBERSORT algorithm, utilizing an R script obtained directly from the CIBERSORT website.[17] The original CIBERSORT gene signature file LM22, which delineates 22 distinct immune cell subtypes, was applied to estimate the proportions of these 22 immune cell types in patients with DM and NPC. To graphically represent the disparities in immune cell infiltration relative to normal controls, we utilized the "ggplot2" package to generate boxplots. Additionally, we performed a correlation analysis to explore the relationships between gene expression and immune cell infiltration.

2.4 | Gene ontology and pathway enrichment analysis

To investigate the underlying commonalities between DM and NPC, GO (Gene Ontology) and KEGG enrichment analyses were conducted on the co-DEGs using the DAVID (https://david.ncifcrf.gov/tools.jsp) online tool.[18,19] KEGG consolidates a vast array of molecular datasets

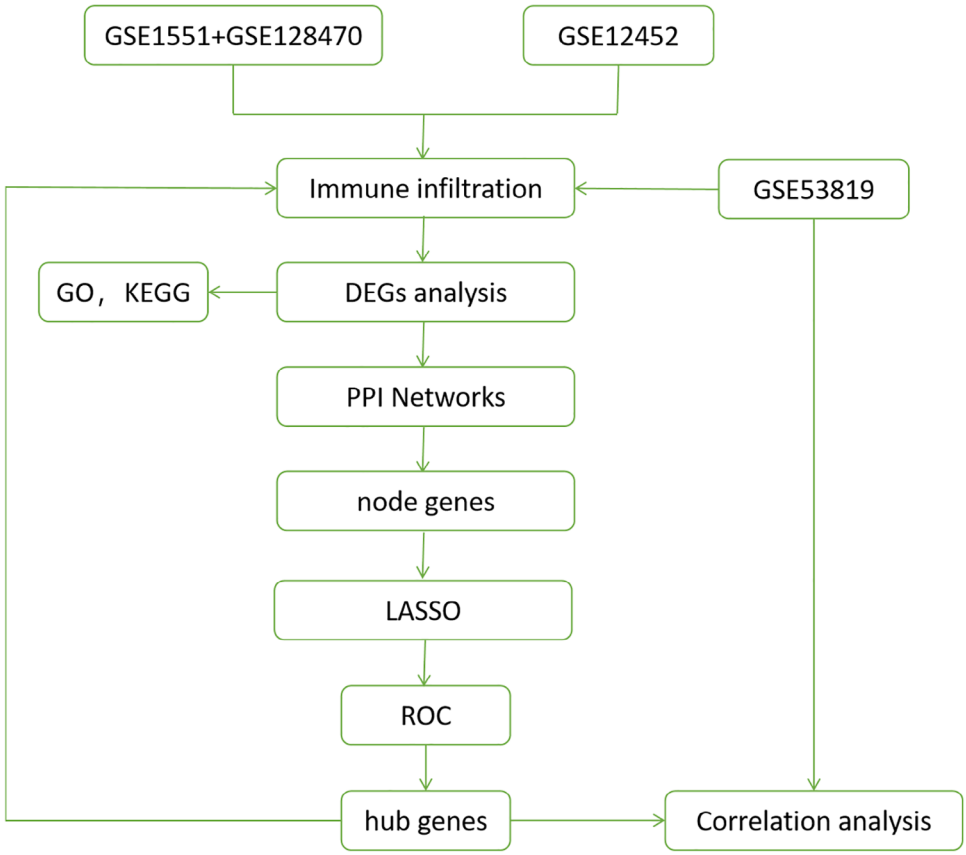

FIGURE 1 The flowchart of the study.

TABLE 1 GEO data set information list.

	GSE1551	GSE128470	GSE12452	GSE53819
Platform	GPL96	GPL96	GPL570	GPL6480
Species	Homo sapiens	Homo sapiens	Homo sapiens	Homo sapiens
Samples in the disease group	13	12	31	18
Samples in the control group	10	12	10	18
Reference	Interferon-alpha/beta-mediated innate immune mechanisms in dermatomyositis	Highly differentiated cytotoxic T cells in inclusion body myositis	Genome-wide expression profiling reveals EBV-associated inhibition of MHC class I expression in NPC	Urokinase-type plasminogen activator receptor signaling is critical in NPC cell growth and metastasis

Abbreviation: NPC, nasopharyngeal carcinoma.

to create comprehensive resources for genome sequencing and other high-throughput experimental methodologies. The GO analysis was primarily focused on molecular function and biological processes. An adjusted $p < 0.05$ was deemed to indicate statistical significance.

2.5 | Protein–protein interaction (PPI) network

The PPI Network plays a pivotal role across the spectrum of life processes. It is integral to biological signaling, regulation of gene expression, metabolism of energy and materials, and modulation of the cell cycle. The PPI network was derived from the STRING (https://cn.string-db.org/) online database,[20,21] employing an interaction score > 0.4. The visualization of the PPI network was accomplished using Cytoscape software. To delineate tightly connected modules within the PPI network, the Molecular Complex Detection (MCODE) plugin[22] was utilized, with parameter settings of a degree cutoff value = 2, a node score cutoff value = 0.2, a K-score = 2, and a maximum depth = 100.

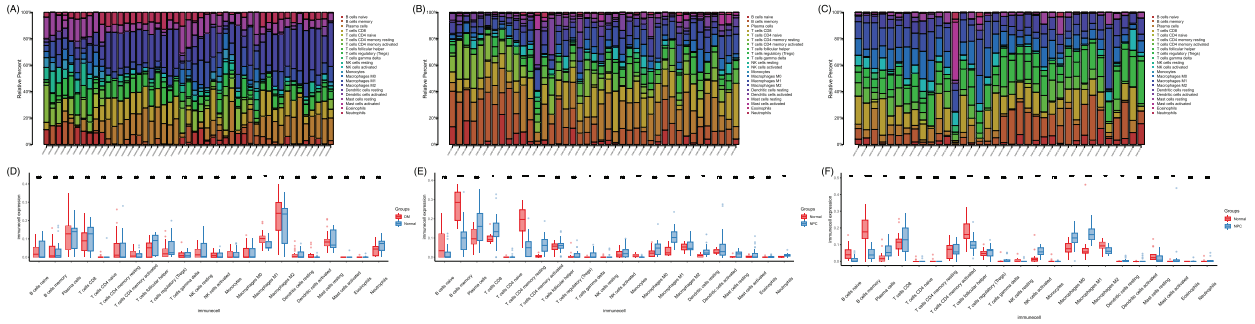

FIGURE 2 Immune infiltration in DM and NPC. Distribution of infiltrating cells in (A) DM, (B) NPC GSE12452 dataset, and (C) NPC GSE53819 dataset. (D) Comparison of immune infiltration between DM group and Normal group. (E) and (F) Comparison of immune infiltration between the Normal group and NPC group. *$p < 0.05$; **$p < 0.01$; ***$p < 0.001$; ****$p < 0.0001$. DM, dermatomyositis; NPC, nasopharyngeal carcinoma; ns, no significant difference.

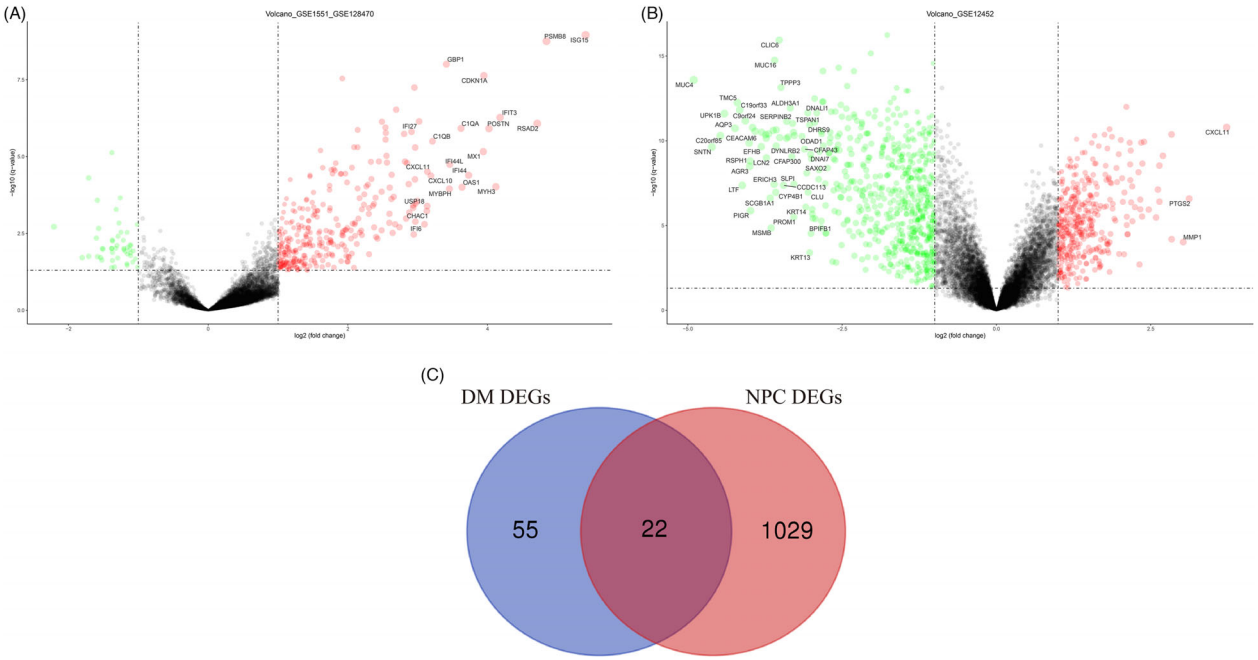

FIGURE 3 Identification of common DEGs in DM and NPC. (A)DEGs Volcano plot between the control and DN samples. The red dots represent up-regulated genes, the black dots represent non-significant genes, and the green dots represent down-regulated genes. (B) DEGs Volcano plot between the control and NPC samples in the GSE12452 dataset. (C) Venn diagrams showing the co-expression in DM and NPC. DEGs, differentially expressed genes; DM, dermatomyositis; NPC, nasopharyngeal carcinoma.

2.6 | Least absolute shrinkage and selection operator (LASSO) regression analysis and receiver operating characteristic (ROC) curve

The "glmnet" package[23] was employed for LASSO regression analysis on the node genes. The diagnostic efficacy of the genes was assessed using the "pROC" package,[24] followed by the construction of diagnostic ROC curves.

2.7 | Statistic analysis

The Wilcoxon rank sum test was implemented for the analysis of immune cell infiltration, the Student's two-tailed *t*-test was applied for gene expression comparisons, and the Spearman's correlation test was employed to evaluate the association between gene expression and cellular immune infiltration. $p < 0.05$ was set for statistical significance.

3 | RESULTS

3.1 | Comparison of immune infiltration between DM and NPC

NPC is one of the most prevalent tumors among patients with DM, a systemic autoimmune disease. We conducted an analysis of immune infiltration in both DM and NPC tissues. The bar chart shows the distribution of infiltrating cells in DM and NPC that we

TABLE 2 Twenty-two co-DEGs.

	DM		NPC	
Gene symbol	logFC	adj.*p*-Val	logFC	adj.*p*-Val
PLAAT4	2.288543149	0.018486382	-1.050304721	0.003436259
CXCL11	3.138025177	0.009794204	3.730457597	5.18E-09
IFI27	3.0198365	0.000927913	-1.017940526	0.038137133
DDX60	2.138846632	0.022260372	1.048332823	0.004216381
PRUNE2	2.623576227	0.041454897	-1.28454477	0.000849495
TFRC	-1.587152832	0.04389555	1.153919733	3.16E-06
MYC	2.140432216	0.001142626	1.145891147	0.005516065
CCL2	2.139490708	0.002783526	2.126834452	0.000500378
NNMT	2.559712804	0.006262474	1.023669128	0.02593072
CD14	2.656932364	0.037805063	1.032032416	0.000697856
CD163	2.805218835	0.001283337	1.433586206	2.30E-05
POSTN	4.021084126	0.001109859	2.838323462	0.000879012
IFI44L	3.4591746	0.006675848	1.607954877	0.00678776
CCL8	2.961208898	0.013391284	2.111687483	0.000190932
TNFRSF21	2.264096801	0.020371399	-1.408417445	0.0004879
ASNS	2.818297999	0.006214282	1.387303655	1.32E-06
C1QB	3.211792771	0.002003079	1.431462197	0.000381173
CXCL10	3.189649788	0.011129316	2.837604958	9.06E-09
RSAD2	4.711143625	0.000967149	1.682661685	0.003377339
IFIH1	2.952422025	0.000119577	1.409607934	7.04E-05
IFI44	3.4591746	0.006675848	1.607954877	0.00678776
IFIT3	4.179020881	0.000847321	1.911128979	9.42E-05

Abbreviations: adj. *p*-Val, adjust *p*-value; DEGs, differentially expressed genes; DM, dermatomyositis; FC, fold change; NPC, nasopharyngeal carcinoma.

analyzed (Figure 2A–C). Box plots revealed that only macrophage M1 were significantly higher in DM compared to the normal control group (Figure 2D). In both NPC datasets, B cells memory was significantly lower, while macrophages M1 and DCs resting were significantly higher in NPC tissues compared to the normal control group (Figure 2E,F). Based on the results of immune infiltration, we speculate that macrophage M1 infiltration may be one of the factors associated with the increased prevalence of NPC in patients with DM.

3.2 | Identification of common DEGs in DM and NPC

Utilizing the "limma" package for differential analysis on the merged dataset from DM (GSE1551 and GSE128470) and the NPC dataset (GSE12452), we identified 77 DEGs in DM and 1051 DEGs in NPC. The distribution of these DEGs was respectively displayed using volcano plots (Figure 3A,B). Subsequently, we employed a Venn diagram to illustrate the intersection of DEGs between the two diseases, which included 22 co-DEGs (Figure 3C). Details of these 22 co-DEGs identified are given in Table 2.

3.3 | Enrichment analysis and PPI

To explore the potential biological functions of these genes, functional enrichment analysis was performed. The KEGG enrichment results indicated that these genes are primarily enriched in the viral protein interaction with cytokine and cytokine receptors, as well as the cytokine–cytokine receptor interaction pathways (Figure 4A). Furthermore, the GO enrichment analysis indicated that these genes are predominantly involved in biological processes such as response to the virus, defense response to the virus, and chemokine-mediated signaling pathway (Figure 4B). More details of the enriched GO/KEGG pathway are included in Table 3. We input these 22 genes into the STRING database to construct the PPI network. By using the MCODE plug-in of cytoscape software, the 22 genes are further optimized into a gene network module with 11 nodes and 100 edges (Figure 4C).

3.4 | Screening and validation of characteristic genes

After the aforementioned analyses, we identified 11 key node genes. Subsequently, we carried out LASSO regression analysis through the

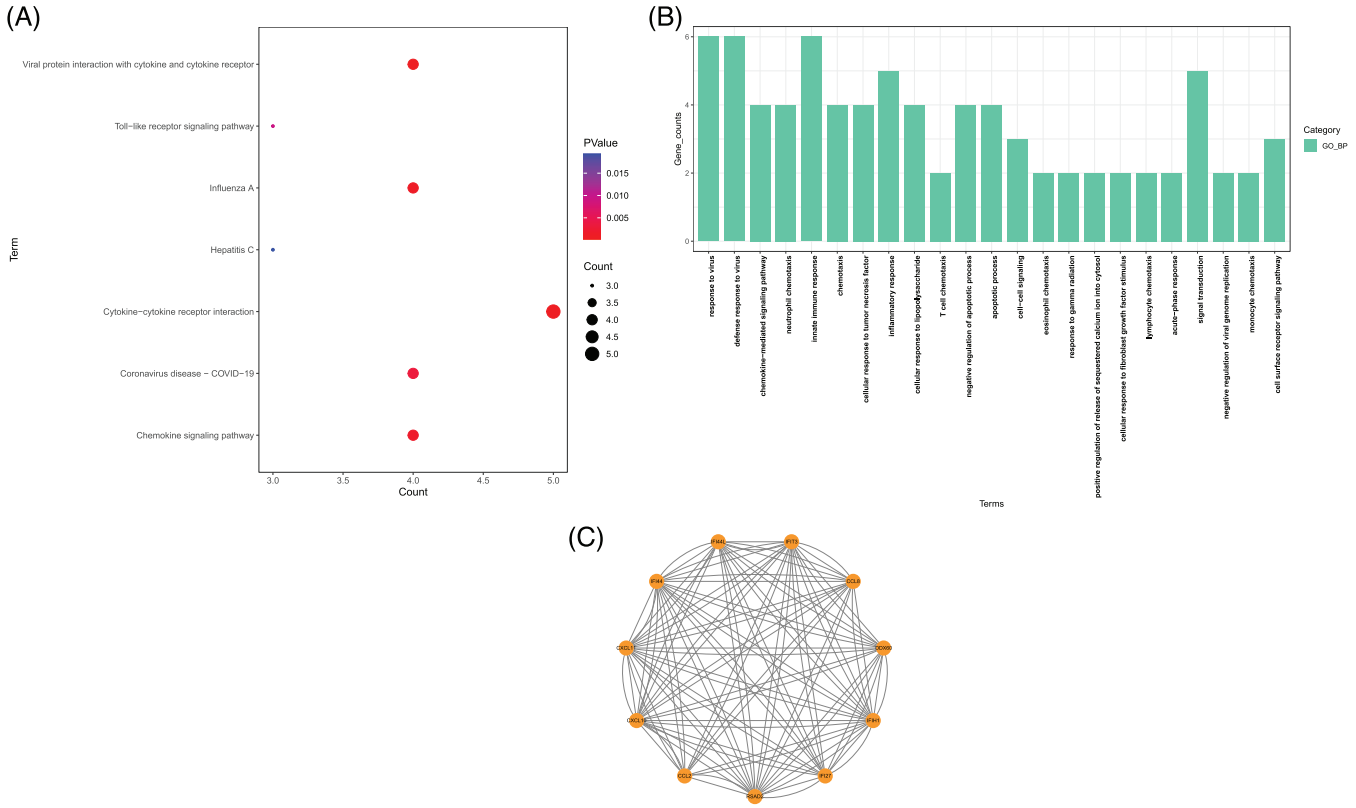

FIGURE 4 Co-DEGs enrichment analysis and PPI. (A) The bubble diagram of the KEGG pathway enrichment analyses of co-DEGs. (B) The bar plot shows the GO-BP enrichment analyses of co-DEGs. (C) The core gene module in co-DEGs. DEG, differentially expressed genes; GO-BP, gene ontology biological process; KEGG, Kyoto encyclopedia of genes and genomes.

"glmnet" package to refine this gene set. This process culminated in the selection of six characteristic genes (Figure 5A,B). We then corroborated the expression of these six genes using data from the GSE53819 dataset. Aside from IFI27, the expression profiles of the other five genes aligned with those from the GSE12452 dataset (Figure 5C). Intriguingly, the expression of IFI27 was notably enhanced in GSE53819 (Figure 5C), in contrast to its diminished expression in GSE12452 (Table 2). Collectively, these observations underscore the pronounced heterogeneity in IFI27 expression within NPC samples.

3.5 | Establishment of characteristic gene ROC curve

Utilizing the "pROC" R package, we conducted an analysis of the characteristic genes CCL2, CCL8, IFIH1, CXCL10, and CXCL11 within the GSE53819 dataset. The ROC curves were constructed to graphically represent the diagnostic performance of these genes. The area under the ROC curve (AUC), a pivotal metric in diagnostic studies, serves as a comprehensive measure of both sensitivity and specificity. It is a robust indicator for assessing the diagnostic efficacy of biomarkers. The AUC for CCL2 was 0.73, denoting moderate diagnostic performance. Conversely, AUCs for CCL8, CXCL10, CXCL11, and IFIH1 surpassed 0.85, indicating superior diagnostic capabilities (Figure 6A–E).

3.6 | The correlation between gene expression and immune cell infiltration

In the analysis of immune infiltration in DM and NPC, we analyzed the correlation between the four hub genes with AUC greater than 0.85 and immune infiltrating cells. The findings revealed a significant positive correlation between the aforementioned genes and macrophage M1 infiltration in DM. Similarly, in NPC, a robust positive correlation was observed between these genes and M1 cell infiltration. Consequently, the four characteristic genes identified emerge as prospective diagnostic markers for the early detection of NPC in DM patients (Figure 7A–C).

4 | DISCUSSION

C-C Motif Chemokine Ligand 8 (CCL8), a chemokine belonging to the CC subfamily, exhibits potent chemotactic properties. It modulates the migration of leukocytes by engaging with G protein-coupled receptors (GPCRs).[25] CCL8 is implicated in an array of pathologies, including infectious diseases and neoplasms, potentially influencing their progression by impacting the migration and activation of white blood cells.[26] Specifically, CCL8 facilitates the migration of M2-type

TABLE 3 GO and KEGG pathways.

Ontology	ID	Description	*p*.adjust
GO-BP	GO:0009615	response to virus	9.58E-08
GO-BP	GO:0051607	defense response to virus	4.50E-06
GO-BP	GO:0070098	chemokine-mediated signaling pathway	5.84E-05
GO-BP	GO:0030593	neutrophil chemotaxis	9.71E-05
GO-BP	GO:0045087	innate immune response	2.15E-04
GO-BP	GO:0006935	Chemotaxis	3.50E-04
GO-BP	GO:0071356	cellular response to tumor necrosis factor	4.27E-04
GO-BP	GO:0006954	inflammatory response	9.69E-04
GO-BP	GO:0071222	cellular response to lipopolysaccharide	0.001103217
GO-BP	GO:0010818	T cell chemotaxis	0.014089363
GO-BP	GO:0043066	negative regulation of the apoptotic process	0.016871581
GO-BP	GO:0006915	apoptotic process	0.025690484
GO-BP	GO:0007267	cell-cell signaling	0.025902216
GO-BP	GO:0048245	eosinophil chemotaxis	0.027989541
GO-BP	GO:0010332	response to gamma radiation	0.029051019
GO-BP	GO:0051281	positive regulation of the release of sequestered calcium ions into the cytosol	0.033285901
GO-BP	GO:0044344	cellular response to fibroblast growth factor stimulus	0.034341869
GO-BP	GO:0048247	lymphocyte chemotaxis	0.037503188
GO-BP	GO:0006953	acute-phase response	0.04275016
GO-BP	GO:0007165	signal transduction	0.043720372
GO-BP	GO:0045071	negative regulation of viral genome replication	0.046928112
GO-BP	GO:0002548	monocyte chemotaxis	0.047969883
GO-BP	GO:0007166	cell surface receptor signaling pathway	0.048029188
KEGG	hsa04061	Viral protein interaction with cytokine and cytokine receptor	3.05E-04
KEGG	hsa04060	Cytokine–cytokine receptor interaction	5.39E-04
KEGG	hsa05164	Influenza A	0.001458695
KEGG	hsa04062	Chemokine signaling pathway	0.002034976
KEGG	hsa05171	Coronavirus disease—COVID-19	0.003531252
KEGG	hsa04620	Toll-like receptor signaling pathway	0.009369864
KEGG	hsa05160	Hepatitis C	0.0193547

Abbreviations: GO, gene ontology; GO-BP, gene ontology biological process; KEGG, Kyoto encyclopedia of genes and genomes.

macrophages to the tumor microenvironment, thereby promoting angiogenesis, tumor growth, and metastasis.[27] Elevated iron levels within the tumor microenvironment of colorectal cancer patients have been shown to stimulate the production of macrophage-derived CCL8 chemokines, which correlates with an unfavorable prognosis.[28] Additionally, the deletion of macrophage-specific Suppressor of Cytokine Signaling 3 (SOCS3) may attenuate tumor-related mortality and metastasis through the mediation of CCL8.[29]

Interferon Induced With Helicase C Domain 1 (IFIH1), synonymously referred to as Melanoma Differentiation-Associated Protein 5 (MDA5), is a cytoplasmic receptor integral to the innate immune system. It is capable of recognizing long double-stranded RNAs (dsRNAs) generated during viral replication.[30] IFIH1 has been characterized as a nucleic acid signaling receptor implicated in various types of cancer. For instance, in colon cancer cells, a reduction in Insulin-like Growth Factor 1 Receptor (IGF-1R) can initiate MDA5-dependent mitochondrial apoptosis.[31] In the context of gliomas, the circular RNA circSOBP has been shown to activate the MDA5-mediated IKKε/TBK1/IRF3 signaling cascade, leading to an upregulation of interferon-I (IFN-I) levels and a consequent enhancement of cellular immune responses.[32]

C-X-C Motif Chemokine Ligand 10 (CXCL10) and C-X-C Motif Chemokine Ligand 11 (CXCL11), as members of the CXC chemokine

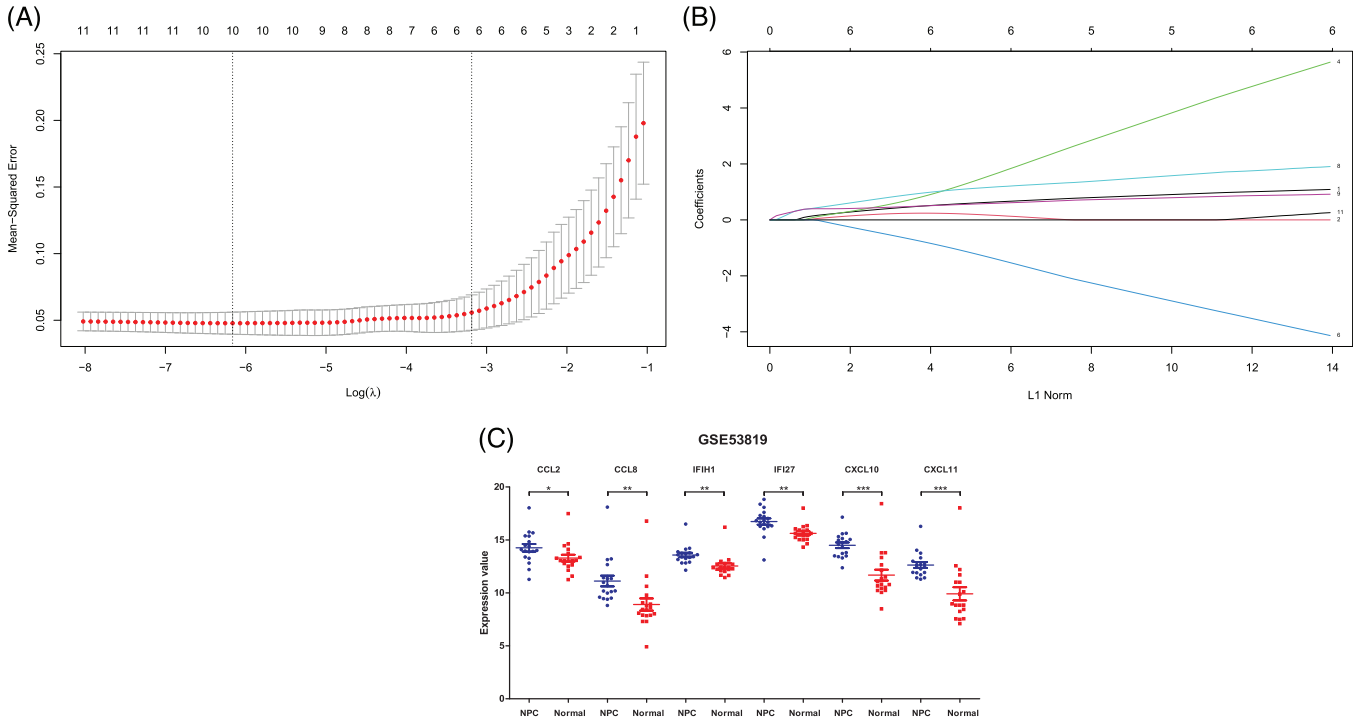

FIGURE 5 Characteristic gene screening and validating. (A) and (B) Results of LASSO regression analysis and six genes were obtained. (C) The expression of these 6 characteristic genes in the GSE53819 dataset. ***$p < 0.001$; **$p < 0.01$; *$p < 0.05$. LASSO, least absolute shrinkage, and selection operator.

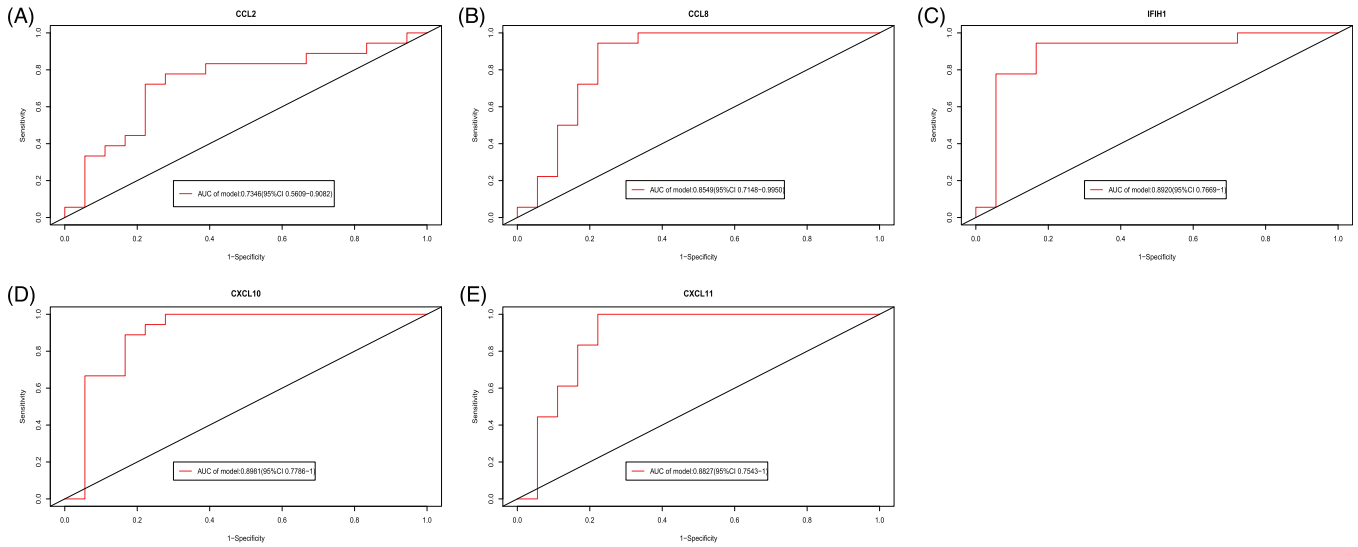

FIGURE 6 ROC curve of the characteristic genes from the GSE53819 dataset. (A–E) ROC curve of the characteristic genes in NPC samples. AUC, the area under the ROC curve; CI, confidence interval; NPC, nasopharyngeal carcinoma; ROC, receiver operating characteristic.

subfamily, bind to the CXCR3 receptor to induce chemotaxis.[33] CXCL10 deficiency has been reported to limit macrophage infiltration, preserve lung stroma, and promote lung growth in bronchopulmonary dysplasia patients.[34] This chemokine is secreted by macrophages and activates them,[34] attracting them into tissues where it regulates inflammatory infiltration and tissue/stromal homeostasis.[35] In colorectal cancer, KRT17 enhances the ubiquitination and degradation of YTHDF2, reducing m6A methylation of CXCL10, which in turn promotes T lymphocyte infiltration.[36] In hepatocellular carcinoma, tumor-associated fibroblasts abnormally secrete CXCL11, which increases IFIH1 and IFIH3 levels, promoting tumor cell migration.[37] In non-small cell lung cancer with the KRAS-G12D mutation, the combination of PD-L1 inhibitors and paclitaxel significantly enhances CD8+ TIL recruitment by upregulating CXCL10/CXCL11 levels, improving treatment

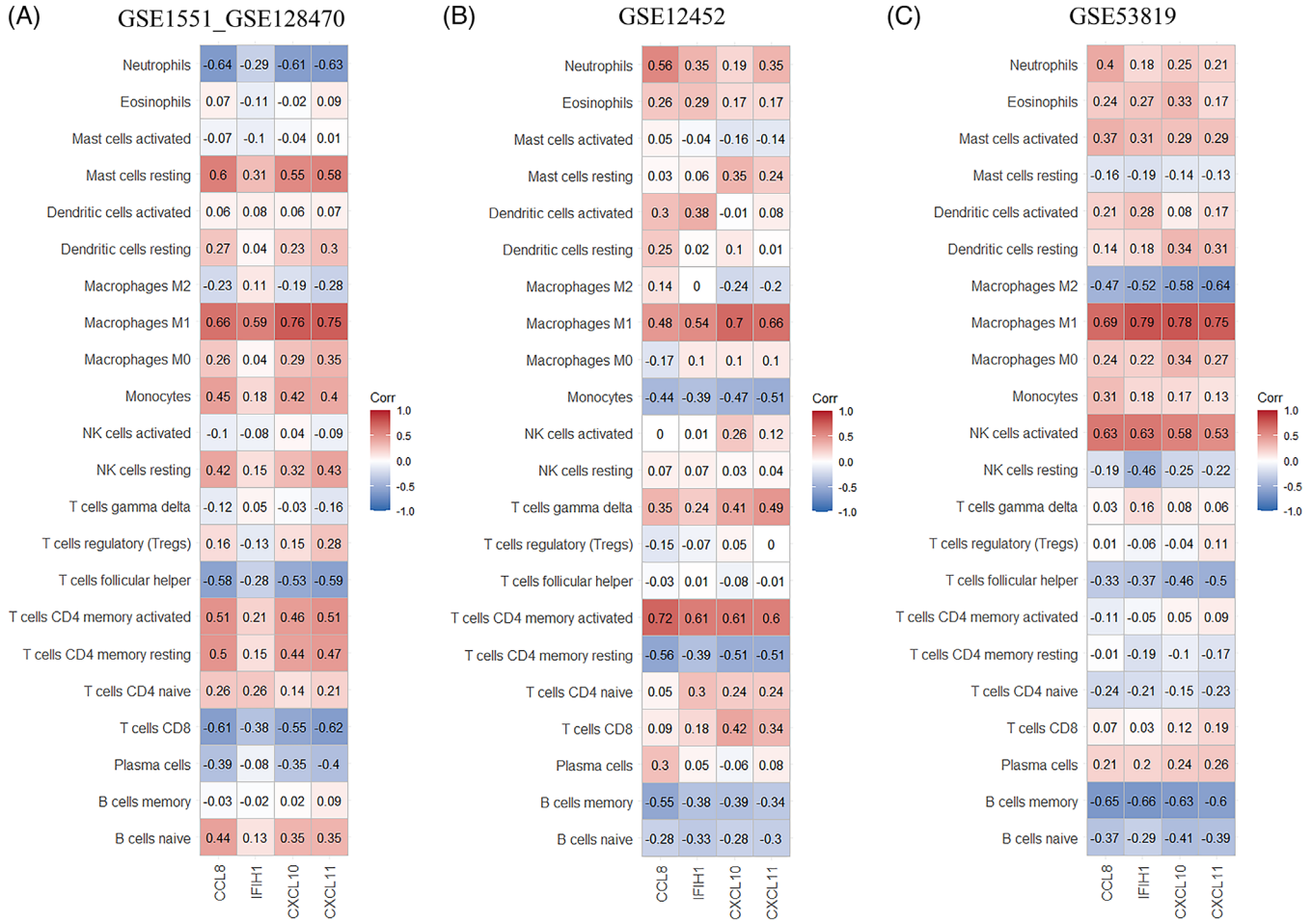

FIGURE 7 Correlation between hub gene and immune infiltration. (A) Correlation between hub gene and immune infiltration in DM. (B) Correlation between hub gene and immune infiltration in NPC GSE12452 dataset. (C) Correlation between hub gene and immune infiltration in NPC GSE53819 dataset. NPC, nasopharyngeal carcinoma.

efficacy.[38] Colon cancer cells increase CXCL11 secretion, induce RBP-Jκ overexpression, and promote immune invasion by tumor-associated macrophages.[39]

In this research, we identified the genes CCL8, IFIH1, CXCL10, and CXCL11 as characteristic genes. Among these, CCL8, CXCL10, and CXCL11 are under the chemokine family, while IFIH1 is an interferon-related gene. These genes exhibit elevated expression levels in both DM and NPC, suggesting their role as shared risk factors for these two conditions and their significance in the pathogenesis of DM and NPC. For DM patients, the expression levels of these characteristic genes can serve as a potentially predictive indicator for the presence of NPC. This study provides a foundation for delving into the intricate relationship between these characteristic genes and the clinical manifestations of the patients. Such exploration is instrumental in enhancing the predictive capabilities of disease diagnostics.

The immune microenvironment and tumor immune microenvironment are burgeoning areas of research and are considered promising therapeutic targets for individuals with autoimmune diseases and malignancies. This study conducted an analysis of DM and NPC samples, focusing on the presence of immune-infiltrating cells. The findings revealed that the macrophage distribution in DM was notably elevated compared to normal tissues. Conversely, in NPC tissues, the heterogeneity of the tumor led to statistically significant variations in the distribution of various immune-infiltrating cells. Notably, there was a common and significant increase in the presence of M1 macrophages. Due to the lack of data on DM complicated with NPC, our conclusions are inferential. However, it is suggested that M1 macrophage infiltration may represent a critical component in the progression of DM in patients who develop NPC.

Utilizing differential expression analysis, PPI analysis, and regression analysis, we have successfully identified four co-upregulated signature genes. These genes exhibit a significant positive correlation with NPC and possess robust diagnostic efficacy, making them potential biomarkers for NPC diagnosis. Specifically, CCL8, CXCL10, and CXCL11, members of the chemokine family, play a crucial role in the polarization and infiltration of macrophages within the tumor microenvironment. These genes have the capacity to enhance the tumor microenvironment's suitability for tumor cell proliferation and invasion either by modulating macrophage polarization or by inhibiting other immune effector cells. The interferon-related gene IFIH1,

also known as MDA5, is recognized in various autoimmune diseases, and anti-MDA5-positive DM constitutes a significant DM subgroup.[40] However, there is a lack of clear evidence linking MDA5 to paraneoplastic tumors associated with DM. The results of enrichment analysis suggest a close relationship between interferon family genes and viral infection processes, highlighting the importance of EBV infection in NPC pathogenesis.[4] The potential involvement of EBV in NPC among DM patients warrants further investigation.

Ultimately, the present study has several inherent limitations. Initially, the research data were sourced from a disparate array of studies within a public database, which could introduce variances that may influence the outcomes. Additionally, the heterogeneity in detection methodologies across different data sources could have introduced biases, potentially skewing the outcomes.

5 | CONCLUSIONS

In summary, our data analysis has pinpointed the signature genes CCL8, IFIH1, CXCL10, and CXCL11 as risk factors for both DM and NPC. These genes are linked to the recruitment of macrophage M1 within the immune microenvironment and demonstrate a strong correlation with the incidence of NPC. They exhibit considerable diagnostic potential and may serve as predictive biomarkers for the development of NPC in DM patients.

ACKNOWLEDGMENTS

The authors would like to express their gratitude to the generous contributors of the GEO database for sharing their valuable data.

CONFLICT OF INTEREST STATEMENT

The authors declare that they have no conflict of interest.

DATA AVAILABILITY STATEMENT

The data that support the findings of this study are available in the GEO database at https://www.ncbi.nlm.nih.gov/gds/?term = . These data were derived from the following resources available in the public domain:—GSE1551, https://www.ncbi.nlm.nih.gov/geo/query/acc.cgi?acc = GSE1551 - GSE128470, https://www.ncbi.nlm.nih.gov/geo/query/acc.cgi?acc = GSE128470 - GSE12452, https://www.ncbi.nlm.nih.gov/geo/query/acc.cgi?acc = GSE12452 - GSE53819, https://www.ncbi.nlm.nih.gov/geo/query/acc.cgi?acc = GSE53819

REFERENCES

1. Cobos GA, Femia A, Vleugels RA. Dermatomyositis: an update on diagnosis and treatment. *Am J Clin Dermatol*. 2020;21(3):339-353.
2. Liu Y, Xu L, Wu H, et al. Characteristics and predictors of malignancy in dermatomyositis: Analysis of 239 patients from northern China. *Oncol Lett*. 2018;16(5):5960-5968.
3. Marzęcka M, Niemczyk A, Rudnicka L. Autoantibody markers of increased risk of malignancy in patients with dermatomyositis. *Clin Rev Allergy Immunol*. 2022;63(2):289-296.
4. Tsao SW, Tsang CM, Lo KW. Epstein-Barr virus infection and nasopharyngeal carcinoma. *Philos Trans R Soc Lond B Biol Sci*. 2017;372(1732):20160270.
5. Ka-Yue CL, Lai-Shun Chung D, Tao L, et al. Epigenomic landscape study reveals molecular subtypes and EBV-associated regulatory epigenome reprogramming in nasopharyngeal carcinoma. *EBioMedicine*. 2022;86:104357.
6. Huang H, Yao Y, Deng X, et al. Immunotherapy for nasopharyngeal carcinoma: current status and prospects (Review). *Int J Oncol*. 2023;63(2):97.
7. Le QT, Colevas AD, O'Sullivan B, et al. Current treatment landscape of nasopharyngeal carcinoma and potential trials evaluating the value of immunotherapy. *J Natl Cancer Inst*. 2019;111(7):655-663.
8. Guo X, Cui J, Yuan X, et al. Long-term trends of nasopharyngeal carcinoma mortality in China from 2006 to 2020 by region and sex: an age-period-cohort analysis. *BMC Public Health*. 2023;23(1):2057.
9. Mebazâa A, Boussen H, Nouira R, et al. Dermatomyositis and malignancy in Tunisia: a multicenter national retrospective study of 20 cases. *J Am Acad Dermatol*. 2003;48(4):530-534./bib>
10. Lau L, Huang L, Fu E, Tan TC, Kong KO, Lim MY. Nasopharyngeal carcinoma in dermatomyositis. *Clin Otolaryngol*. 2021;46(5):1082-1088.
11. Bai R, Sun J, Xu Y, Sun Z, Zhao X. Incidence and mortality trends of nasopharynx cancer from 1990 to 2019 in China: an age-period-cohort analysis. *BMC Public Health*. 2022;22(1):1351.
12. Liu T, Liu JP. Integration analysis of single-cell transcriptome reveals specific monocyte subsets associated with melanoma brain and leptomeningeal metastasis. *Skin Res Technol*. 2024;30(4):e13710.
13. Barrett T, Wilhite SE, Ledoux P, et al. NCBI GEO: archive for functional genomics data sets—update. *Nucleic Acids Res*. 2013;41(Database issue):D991-D995.
14. Davis S, Meltzer PS. GEOquery: a bridge between the Gene Expression Omnibus (GEO) and BioConductor. *Bioinformatics*. 2007;23(14):1846-1847.
15. Ritchie ME, Phipson B, Wu D, et al. limma powers differential expression analyses for RNA-sequencing and microarray studies. *Nucleic Acids Res*. 2015;43(7):e47.
16. Ma Y, Lai J, Wan Q, et al. Identification of common mechanisms and biomarkers for dermatomyositis and atherosclerosis based on bioinformatics analysis. *Skin Res Technol*. 2024;30(6):e13808.
17. Chen B, Khodadoust MS, Liu CL, Newman AM, Alizadeh AA. Profiling tumor infiltrating immune Cells with CIBERSORT. *Methods Mol Biol*. 2018;1711:243-259.
18. da Huang D, Sherman BT, Lempicki RA. Systematic and integrative analysis of large gene lists using DAVID bioinformatics resources. *Nat Protoc*. 2009;4(1):44-57.
19. Sherman BT, Hao M, Qiu J, et al. DAVID: a web server for functional enrichment analysis and functional annotation of gene lists (2021 update). *Nucleic Acids Res*. 2022;50(W1):W216-W221.
20. Szklarczyk D, Kirsch R, Koutrouli M, et al. The STRING database in 2023: protein-protein association networks and functional enrichment analyses for any sequenced genome of interest. *Nucleic Acids Res*. 2023;51(D1):D638-D646.
21. von Mering C, Huynen M, Jaeggi D, Schmidt S, Bork P, Snel B. STRING: a database of predicted functional associations between proteins. *Nucleic Acids Res*. 2003;31(1):258-261.
22. Bandettini WP, Kellman P, Mancini C, et al. MultiContrast Delayed Enhancement (MCODE) improves detection of subendocardial myocardial infarction by late gadolinium enhancement cardiovascular magnetic resonance: a clinical validation study. *J Cardiovasc Magn Reson*. 2012;14(1):83.
23. Friedman J, Hastie T, Tibshirani R. Regularization paths for generalized linear models via coordinate descent. *J Stat Softw*. 2010;33(1):1-22.
24. Robin X, Turck N, Hainard A, et al. pROC: an open-source package for R and S+ to analyze and compare ROC curves. *BMC Bioinformatics*. 2011;12:77.
25. Hughes CE, Nibbs RJB. A guide to chemokines and their receptors. *FEBS J*. 2018;285(16):2944-2971.

26. Korbecki J, Kojder K, Simińska D, et al. CC chemokines in a tumor: a review of pro-cancer and anti-cancer properties of the ligands of receptors CCR1, CCR2, CCR3, and CCR4. *Int J Mol Sci*. 2020;21(21):8412.
27. Farmaki E, Kaza V, Chatzistamou I, Kiaris H. CCL8 promotes postpartum breast cancer by recruiting M2 macrophages. *iScience*. 2020;23(6):101217.
28. Yamane T, Kanamori Y, Sawayama H, et al. Iron accelerates Fusobacterium nucleatum-induced CCL8 expression in macrophages and is associated with colorectal cancer progression. *JCI Insight*. 2022;7(21):e156802.
29. Hiwatashi K, Tamiya T, Hasegawa E, et al. Suppression of SOCS3 in macrophages prevents cancer metastasis by modifying macrophage phase and MCP2/CCL8 induction. *Cancer Lett*. 2011;308(2):172-180.
30. del Toro Duany Y, Wu B, Hur S. MDA5-filament, dynamics and disease. *Curr Opin Virol*. 2015;12:20-25.
31. Wang SQ, Yang XY, Yu XF, Cui SX, Qu XJ. Knockdown of IGF-1R triggers viral RNA sensor MDA5- and RIG-I-mediated mitochondrial apoptosis in colonic cancer cells. *Mol Ther Nucleic Acids*. 2019;16:105-117.
32. Mu M, Niu W, Chu F, Dong Q, Hu S, Niu C. CircSOBP suppresses the progression of glioma by disrupting glycolysis and promoting the MDA5-mediated immune response. *iScience*. 2023;26(10):107897.
33. Tokunaga R, Zhang W, Naseem M, et al. CXCL9, CXCL10, CXCL11/CXCR3 axis for immune activation—a target for novel cancer therapy. *Cancer Treat Rev*. 2018;63:40-47.
34. Hirani DV, Thielen F, Mansouri S, et al. CXCL10 deficiency limits macrophage infiltration, preserves lung matrix, and enables lung growth in bronchopulmonary dysplasia. *Inflamm Regen*. 2023;43(1):52.
35. Tsai CF, Chen JH, Yeh WL. Pulmonary fibroblasts-secreted CXCL10 polarizes alveolar macrophages under pro-inflammatory stimuli. *Toxicol Appl Pharmacol*. 2019;380:114698.
36. Liang W, Liu H, Zeng Z, et al. KRT17 promotes T-lymphocyte infiltration through the YTHDF2-CXCL10 axis in colorectal cancer. *Cancer Immunol Res*. 2023;11(7):875-894.
37. Liu G, Sun J, Yang ZF, et al. Cancer-associated fibroblast-derived CXCL11 modulates hepatocellular carcinoma cell migration and tumor metastasis through the circUBAP2/miR-4756/IFIT1/3 axis. *Cell Death Dis*. 2021;12(3):260.
38. Liu C, Zheng S, Wang Z, et al. KRAS-G12D mutation drives immune suppression and the primary resistance of anti-PD-1/PD-L1 immunotherapy in non-small cell lung cancer. *Cancer Commun*. 2022;42(9):828-847.
39. Liu M, Fu X, Jiang L, et al. Colon cancer cells secreted CXCL11 via RBP-Jκ to facilitated tumour-associated macrophage-induced cancer metastasis. *J Cell Mol Med*. 2021;25(22):10575-10590.
40. Kurtzman D, Vleugels RA. Anti-melanoma differentiation-associated gene 5 (MDA5) dermatomyositis: a concise review with an emphasis on distinctive clinical features. *J Am Acad Dermatol*. 2018;78(4):776-785.

How to cite this article: Kai J, Huang H, Su J, Chen Q. Identification of shared immune infiltration characteristic molecules in dermatomyositis and nasopharyngeal carcinoma using bioinformatics. *Skin Res Technol*. 2024;30:e13871. https://doi.org/10.1111/srt.13871